Controlled Synthesis and Luminescence of Lanthanide Doped $NaYF_4$ Nanocrystals

Leyu Wang[†,§] and Yadong Li*[,†]

Department of Chemistry, Tsinghua University Beijing, 100084 P. R. China, and College of Chemistry and Materials Science, Anhui Key Laboratory of Functional Molecular Solids, Anhui Normal University, Wuhu, 241000 P. R. China

Received August 10, 2006. Revised Manuscript Received November 9, 2006

A range of nearly monodispersed $NaYF_4$ single-crystal nanorods, hexagonal nanoplates, and nanoparticles have been successfully prepared via a facile wet chemical technology. Varying the dopants leads to different luminescence. These as-prepared nanocrystals not only present novel room-temperature downconversion (DC) and upconversion (UC) fluorescence but can also be transparently dispersed in cyclohexane. The effects of reaction temperature and time, doped ion concentration, ratio of NaF to $Ln(NO_3)_3$, and the reactant content on the shape, size, and crystal phase purity of the as-prepared nanocrystals have been investigated in detail. The fluorescence photos, spectra, luminescence mechanism, and the formation mechanism of the nanorods have also been demonstrated. For the next biolabel applications, the colloidal nanoparticles dispersed in cyclohexane have also been transferred into water by surface silane modification. For their unique DC and UC luminescence and high processability, these nanocrystals will open new avenues in biolabels, light-emitting diodes (LEDs), color displays, anticounterfeiting, and solid-state lasers.

Introduction

Recently, luminescent nanomaterials have attracted a great deal of interest for their potential applications such as color displays,[1,2] field-effect transistors (FET),[3,4] optoelectronics,[5] medical and biological labels,[6−11] solar cells,[12−14] and as a light source in lasers.[15,16] Among these luminescent nanomaterials, semiconductor nanomaterials have great advantages than the organic dyes and have drawn notable attentions; however, they also suffer from photobleaching before necessary surface modification. On the other hand, UV excitation will cause damage to the biological tissues and strong background fluorescence and further affect the sensitivity of the assay method when the materials are used as in vivo biolabels.[17−19] Hence, it is important to search for a new kind of phosphors with controllable size and shape, high crystallinity, high room-temperature quantum yields, and tunable emissions. Lanthanide-doped luminescence materials[17−26] have drawn great attention and played an outstanding role in the above fields for their novel downconversion (DC)[19,22−24] as well as upconversion (UC)[17−20,26] fluorescence, which make them efficient complementarities and companions to semiconductors and dyes.

Photon upconversion in lanthanide-doped materials[14,17−20,25−28] has been investigated intensively because of the possibility of infrared-pumped visible lasers and their

* To whom correspondence should be addressed. Fax: 86 10-6278-8765. E-mail: ydli@tsinghua.edu.cn.
† Tsinghua University.
§ Anhui Normal University.

(1) Lee, M. H.; Oh, S. G.; Yi, S. C.; Seo, D. S.; Hong, J. P.; Kim, C. O.; Yoo, Y. K.; Yoo, J. S. *J. Electrochem. Soc.* **2000**, *147*, 3139.
(2) Wang, Q. H.; Setlur, A. A.; Lauerhaas, J. M.; Dai, J. Y.; Seelig, E. W.; Chang, R. P. H. *Appl. Phys. Lett.* **1998**, *72*, 2912.
(3) Sun, B.; Sirringhaus, H. *Nano Lett.* **2005**, *5*, 2408.
(4) Talapin, D. V.; Murray, C. B. *Science* **2005**, *310*, 86.
(5) Huang, Y.; Lieber, C. M. *Pure Appl. Chem.* **2004**, *76*, 2051.
(6) Bruchez, M.; Moronne, M.; Gin, P.; Weiss, S.; Alivisatos, A. P. *Science* **1998**, *281*, 2013.
(7) Chan, W. C. W.; Nie, S. M. *Science* **1998**, *281*, 2016.
(8) Gao, X. H.; Cui, Y. Y.; Levenson, R. M.; Chung, L. W. K.; Nie, S. M. *Nat. Biotechnol.* **2004**, *22*, 969.
(9) Medintz, I. L.; Uyeda, H. T.; Goldman, E. R.; Mattoussi, H. *Nat. Mater.* **2005**, *4*, 435.
(10) Santra, S.; Xu, J. S.; Wang, K. M.; Tan, W. H. *J. Nanosci. Nanotechnol.* **2004**, *4*, 590.
(11) Wang, L.; Yang, C. Y.; Tan, W. H. *Nano Lett.* **2005**, *5*, 37.
(12) Liu, J. F.; Yao, Q. H.; Li, Y. D. *Appl. Phys. Lett.* **2006**, *88*.
(13) Law, M.; Greene, L. E.; Johnson, J. C.; Saykally, R.; Yang, P. D. *Nat. Mater.* **2005**, *4*, 455.
(14) Shalav, A.; Richards, B. S.; Trupke, T.; Kramer, K. W.; Gudel, H. U. *Appl. Phys. Lett.* **2005**, *86*.
(15) Choi, H. J.; Johnson, J. C.; He, R. R.; Lee, S. K.; Kim, F.; Pauzauskie, P.; Goldberger, J.; Saykally, R. J.; Yang, P. D. *J. Phys. Chem. B* **2003**, *107*, 8721.
(16) Johnson, J. C.; Choi, H. J.; Knutsen, K. P.; Schaller, R. D.; Yang, P. D.; Saykally, R. J. *Nat. Mater.* **2002**, *1*, 106.
(17) Wang, L. Y.; Yan, R. X.; Hao, Z. Y.;Wang, L.; Zeng, J. H.; Bao, J.; Wang, X.; Peng, Q.; Li, Y. D. *Angew. Chem., Int. Ed.* **2005**, *44*, 6054.
(18) Yi, G. S.; Lu, H. C.; Zhao, S. Y.; Yue, G.; Yang, W. J.; Chen, D. P.; Guo, L. H. *Nano Lett.* **2004**, *4*, 2191.
(19) Wang, L. Y.; Li, Y. D. *Chem. Commun.* **2006**, *16*, 2557.
(20) Heer, S.; Kompe, K.; Gudel, H. U.; Haase, M. *Adv. Mater.* **2004**, *16*, 2102.
(21) Heer, S.; Lehmann, O.; Haase, M.; Gudel, H. U. *Angew. Chem. Int. Ed.* **2003**, *42*, 3179.
(22) Meiser, F.; Cortez, C.; Caruso, F. *Angew. Chem., Int. Ed.* **2004**, *43*, 5954.
(23) Riwotzki, K.; Meyssamy, H.; Kornowski, A.; Haase, M. *J. Phys. Chem. B* **2000**, *104*, 2824.
(24) Riwotzki, K.; Meyssamy, H.; Schnablegger, H.; Kornowski, A.; Haase, M. *Angew. Chem., Int. Ed.* **2001**, *40*, 573.
(25) Yan, R. X.; Li, Y. D. *Adv. Funct. Mater.* **2005**, *15*, 763.
(26) Zeng, J. H.; Su, J.; Li, Z. H.; Yan, R. X.; Li, Y. D. *Adv. Mater.* **2005**, *17*, 2119.
(27) Sivakumar, R.; van Veggel, F.; Raudsepp, M. *J. Am. Chem. Soc.* **2005**, *127*, 12464.
(28) van de Rijke, F.; Zijlmans, H.; Li, S.; Vail, T.; Raap, A. K.; Niedbala, R. S.; Tanke, H. J. *Nat. Biotechnol.* **2001**, *19*, 273.

10.1021/cm061887m CCC: $37.00
Published on Web 01/20/2007

potential applications in color display, optical storage, solar cell, and biolabels. Their unique upconversion luminescence mechanism, that is, emitting visible light (blue-green-red) by absorbing two or three photons of near-infrared (NIR) light (excitation, low energy), makes them especially suitable for ideal biolabels for the following reasons.[17−20,28] First, unlike the UV excitation source (high energy) usually used in organic dye and semiconductor biolabels, the low exciting energy (NIR light) for upconversion phosphors is only weakly absorbed by biological tissue, which will cause no damage to the biological samples. Second, the biological tissues have no upconversion ability and the excitation in the NIR induces only a very weak autofluorescence background, which thus increase the sensitivity of the assays. Third, the lanthanide ion is embedded in an inorganic matrix, yielding long luminescence lifttimes, high quantum efficiencies, and photostability; the upconversion process of the lanthanide-doped inorganic nanomaterials are mainly located in the lattice of the host materials and almost not affected by the outside environments, which further makes them suitable for tagging in complicated biological systems.

To date, there have been a number of reports in the literature about upconversion luminescence materials. To the best of our knowledge, among the reported upconversion materials, hexagonal phase $NaYF_4$ is one of the most efficient upconversion host materials for visible upconversion fluorescence.[17,19,26] Most of these studies about $NaYF_4$, however, have been performed on dried powder materials. Moreover, to obtain the pure hexagonal phase $NaYF_4$ (whose upconversion efficiency is far higher than that of the cubic phase), researchers often adopted a high-temperature treatment in the reported literature, which in reverse suffered from unreasonable control of the size, shape, and redispersibility of the as-prepared materials.[29,30] For any imaging or display applications based on the upconversion principle in a fluid, especially for biolabels, the prerequisite is redispersing the nanomaterials in a transparent colloidal solution. So, besides good crystallinity, a reasonable particle size distribution is required, and the particles have to possess proper surface properties to ensure colloidal redispersibility. In recent years, some new synthesis methods have been reported for monodisperse $NaYF_4$ nanoparticles with cubic phase;[18,20,31,32] however, the hexagonal phase $NaYF_4$ nanocrystals with controllable size and morphology has not successfully been achieved. Therefore, it is still a challenge to develop a facile technology to prepare hexagonal phase $NaYF_4$ nanocrystals with uniform shape and size, high luminescence, and good redispersibility. Recently, a facile method for the preparation of hexagonal phase $NaYF_4$ single-crystal nanorods with strong luminescence has been reported.[33] In the present work, we detailedly demonstrated the effects of different experimental conditions on the size, morphology, and crystal phase purity of the $NaYF_4$ nanoparticles, nanorods, and nanoplates. Moreover, the novel down- and up-conversion fluorescence and luminescence mechanism have been demonstrated. We also make some preliminary discussion on the formation mechanism of the nanorods. For the next biolabel application, the colloidal nanoparticles dispersed in cyclohexane have been transferred into water by surface silanization modification.

(29) Martin, N.; Boutinaud, P.; Mahiou, R.; Cousseinsa, J. C.; Bouderbal, M. *J. Mater. Chem.* **1999**, *9*, 125.
(30) Menyuk, N.; Dwight, K.; Pierce, J. W. *Appl. Phys. Lett.* **1972**, *21*, 159.
(31) Mai, H. X.; Zhang, Y. W.; Si, R.; Yan, Z. G.; Sun, L. D.; You, L. P.; Yan, C. H. *J. Am. Chem. Soc.* **2006**, *128*, 6426.
(32) Wang, X.; Zhuang, J.; Peng, Q.; Li, Y. D. *Nature* **2005**, *437*, 121.
(33) Wang, L. Y.; Li, Y. D. *Nano Lett.* **2006**, *6*, 1645.

Materials and Methods

Chemicals. All the chemicals were of analytical grade and used as received without further purification. Deionized water was used throughout. $Y(NO_3)_3{\cdot}6H_2O$, $Tm(NO_3)_3{\cdot}6H_2O$, $Er(NO_3)_3{\cdot}6H_2O$, $Yb(NO_3)_3{\cdot}6H_2O$, Eu $(NO_3)_3{\cdot}6H_2O$, and $Tb(NO_3)_3{\cdot}6H_2O$ (purity >99.9%) were purchased from the Shanghai Chemical Reagent Company. NaF, NaOH, and HNO_3 were supplied by the Beijing Chemical Reagent Company.

Solvothermal Synthesis of $NaYF_4$ Nanocrystals. These nanocrystals have been prepared by adapting our recently reported LSS synthetic strategy.[32] Detailed synthetic methods of the $NaYF_4$ nanocrystals have been summarized in the tables of this work.

Powder X-ray Diffraction (XRD). The crystallinity and phase purity of the products were examined via XRD using a Brucker D8-advance X-ray diffractometer with Cu Kα radiation ($\lambda = 1.5418$ Å), keeping the operating voltage and current at 40 kV and 40 mA, respectively. The 2θ range used was from 10 to 70° in steps of 0.02°, with a count time of 2 s.

Transmission Electron Microscopy (TEM). The size and morphology of the products were observed by using the JEOL JEM-1200EX transmission electron microscope with a tungsten filament at an accelerating voltage of 100−120 kV. Samples were prepared by placing a drop of a dilute cyclohexane dispersion of the nanocrystals on the surface of a copper grid. High-resolution transmission electron microscopy (HRTEM) images are obtained on a JEOL JEM-2010F transmission electron microscope.

Fluorescence Spectroscopy. Downconversion luminescence spectra were recorded with a Hitachi F-4500 fluorescence spectrophotometer. Upconversion fluorescence spectra were obtained on the Hitachi F-4500 fluorescence spectrophotometer with a 0−800 mW adjustable laser (980 nm, Beijing Hi-Tech Optoelectronic Co., China) as the excitation source, instead of the xenon source in the spectrophotometer, and with a fiber optic accessory.

Results and Discussion

The morphology, size, and crystal phase purity of the as-prepared nanocrystals are mainly affected by the following conditions, such as reaction temperature and time, reactant concentration, the doped ion concentration, and the ratio of NaF to $Ln(NO_3)_3$, which has been discussed in detail as follows.

Effect of NaF Concentration. The effects of the NaF content on the morphology, size, and crystal structure of the as-prepared nanocrystals have been studied by changing the content of NaF (1.0 M) from 2.4 mL to 6.0 mL. Table 1 listed the synthetic conditions and the results. Figure 1 depicted the TEM images of the nanocrystals prepared under the conditions listed in Table 1. From Table 1 and Figure 1, it can be seen that the morphology and size of the nanocrystals have been affected by the NaF content. Under the settled conditions, when the ratio of NaF-to-$Ln(NO_3)_3$ (Ln represents the total amount of Y^{3+} and the doped rare earth such as Eu^{3+}, Tb^{3+}, Yb^{3+}/Er^{3+}, or Yb^{3+}/Tm^{3+}) is the

Table 1. Effect of NaF Content on the Nanocrystals[a]

$Y(NO_3)_3$ (0.5 M)	$Eu(NO_3)_3$ (0.5 M)	$Tb(NO_3)_3$ (0.5 M)	NaF (1.0 M)	figure, shape
1.14 mL, 95%	60 μL, 5%		2.4 mL	Figure 1a, irregular nanoparticles, $d \approx 7$ nm
1.14 mL, 95%	60 μL, 5%		3.0 mL	Figure 1b, nanocubes, $d \approx 10-13$ nm
1.14 mL, 95%	60 μL, 5%		6.0 mL	Figure 1c, nanocubes, $d \approx 10-13$ nm
1.14 mL, 95%		60 μL, 5%	2.4 mL	Figure 1d, irregular nanoparticles, $d \approx 7$ nm
1.14 mL, 95%		60 μL, 5%	3.0 mL	Figure 1e, nanocubes, d $\approx 10-13$ nm
1.14 mL, 95%		60 μL, 5%	6.0 mL	Figure 1f, nanocubes, $d \approx 10-13$ nm

[a] 1.2 g of NaOH, 9 mL of H_2O, 7 mL of C_2H_5OH, 20 mL of oleic acid, temperature 160 °C, time 8 h.

Table 2. Effect of Eu^{3+}-Doped Concentration on the Nanocrystals[a]

group	$Y(NO_3)_3$ (0.5 M)	$Eu(NO_3)_3$ (0.5 M)	NaF (1.0 M)	T (°C)	t (h	figure, shape
I	400 μL, 71.4%	160 μL, 28.6%	3 mL	170	24	Figure 3a, nanorods, $d \approx 30$ nm, $l \approx 700-800$ nm
	160 μL, 28.6%	400 μL, 71.4%	3 mL	170	24	Figure 3b, nanorods, $d \approx 7$ nm, $l \approx 110$ nm
II	570 μL, 95%	30 μL, 5%	3 mL	180	48	Figure 3c, nanorods, $d \approx 32$ nm, $l \approx 700-800$ nm
	400 μL, 71.4%	160 μL, 28.6%	3 mL	180	48	Figure 3d, nanorods, $d \approx 30$ nm, $l \approx 450-700$ nm
	160μl, 28.6%	400 μL, 71.4%	3 mL	180	48	Figure 3e, nanorods, $d \approx 7$ nm, $l \approx 80-90$ nm
III	1.9 mL, 95%	100 μL, 5%	4 mL	195	24	Figure 3f, nanorods, $d \approx 180$ nm, $l \approx 350-380$ nm
	0.6 mL, 30%	1.4 mL, 70%	4 mL	195	24	Figure 3g, hexagonal nanoplates, $d \approx 210$ nm

[a] 1.2 g of NaOH, 9 mL of H_2O, 7 mL of C_2H_5OH, 20 mL of oleic acid.

Table 3. Effect of Reactant Concentration on Nanocrystals[a]

$Y(NO_3)_3$ (0.5 M)	$Ln(NO_3)_3$	NaF (1.0 M)	T (°C)	t (h)	figure, shape, and size
160 μL, 28.6%	1.0 mL, 71.4% ($Eu(NO_3)_3$, 0.2M)	3 mL	160	8	Figure 5a, nanorods, $d \approx 10-13$ nm, $l \approx 100-120$ nm
1.14 mL, 95%	60 μL, 5% ($Eu(NO_3)_3$, 0.5M)	3 mL	160	8	Figure 5b, nanocubes, $d = \sim 10-13$ nm
160 μL, 28.6%	1.0 mL, 71.4% ($Tb(NO_3)_3$, 0.2M)	3 mL	160	8	Figure 5c, nanorods, $d \approx 20-25$ nm, $l \approx 230$ nm
1.14 mL, 95%	60 μL, 5% ($Tb(NO_3)_3$, 0.5M)	3 mL	160	8	Figure 5d, nanocubes, $d \approx 10-13$ nm

[a] 1.2 g of NaOH, 9 mL of H_2O, 7 mL of C_2H_5OH, 20 mL of oleic acid.

Table 4. Effect of the Solvothermal Temperature and Time on the $NaYF_4$:Yb^{3+}/Er^{3+} Nanocrystals[a]

$Y(NO_3)_3$ (0.5 M)	$Yb(NO_3)_3$ (0.2 M)	$Er(NO_3)_3$ (0.2 M	NaF (1.0 M)	T (°C)	t (h)	figure, shape
180 μL, 67%	180 μL, 27%	45 μL, 6%	8 mL	210	20	Figure 6a, nanorods, $d \approx 15-20$ nm, $l \approx 100-150$ nm
180 μL, 67%	180 μL, 27%	45 μL, 6%	8 mL	180	20	Figure 6b, manorods, $d \approx 20$ nm, $l \approx 500-600$ nm
180 μL, 67%	180 μL, 27%	45 μL, 6%	8 mL	180	8	Figure 6c, manocubes, $d \approx 10$ nm
1.9 mL, 95%	150 μL, 3%	100 μL, 2%	4 mL	190	24	Figure 6d, manorods, $d \approx 65$ nm, $l \approx 150$ nm
1.9 mL, 95%	150 μL, 3%	100 μL, 2%	8 mL	190	24	Figure 6e, manorods, $d \approx 45$ nm, $l \approx 1200$ nm
950 μL, 95%	75 μL, 3%	50 μL, 2%	8 mL	190	24	Figure 6f, manorods, $d \approx 35$ nm, $l \approx 900$ nm

[a] 1.2 g of NaOH, 5 mL of H2O, 7 mL of C_2H_5OH, 20 mL of oleic acid.

stoichiometric proportion, i.e., four, the as-prepared nanoparticles are irregular, and the particle size is about 7 nm (see Figure 1a for $NaYF_4$:Eu^{3+} and Figure 1d for $NaYF_4$:Tb^{3+}). When the ratio reaches 5, which means the NaF is in a slight excess to $Ln(NO_3)_3$, the particles are regular nanocubes (see Figure 1b for $NaYF_4$:Eu^{3+} and Figure 1e for $NaYF_4$:Tb^{3+}). Meanwhile, the particle size increase to ~10−13 nm. However, when the ratio is further increased to 10, the NaF content has no obvious effect on the morphology and size of the as-synthesized nanocrystals, which can be seen from images c and f of Figure 1. Comparing Figure 1b with Figure 1c, although the NaF content doubled from 3.0 to 6.0 mL, the particle shape and size have no apparent change. In addition, the NaF content has an effect on not only the shape and size but also the crystal structure of the nanoparticles. The X-ray diffraction (XRD) patterns of the as-prepared nanoparticles are demonstrated in Figure 2, and the peaks in the XRD patterns (Figure 2a) of the irregular nanoparticles depicted in Figure 1a matched very well with the standard face-centered cubic $NaYF_4$ crystal structure data (Joint Committee for Powder Diffraction Studies (JCPDS) card 77-2042). Meanwhile, the XRD patterns depicted in Figure 2b confirmed the existence of both cubic (JCPDS card 77-2042) and hexagonal phase $NaYF_4$ (JCPDS card 16-0334); in addition, small amounts of NaF were also found in the XRD patterns of the as-prepared nanocubes depicted in Figure 1b. These elementary results indicated that the NaF content has effects not only on the morphology and size but also on the crystal structure of the as-synthesized nanocrystals. It is noteworthy that the nanocubes of images b, c, e, and f of Figure 1 have the similar XRD patterns, and the XRD pattern of the nanoparticles depicted in Figure 1d is identical to that of Figure 1a.

Effect of Doped Ion Concentration. Besides the effect of NaF contents, the influence of the doped ion concentration also has been taken into account in this work. Here, we use the europium (Eu^{3+})-doped $NaYF_4$ as examples to discuss the effects of the doped ion concentration. The experimental conditions and results are listed in Figure 3 and Table 2. Tto clearly demonstrate the effect of the Eu^{3+} concentration, we divide the results into three groups (see Table 2), i.e. group I (Figure 3a and 3b), II (Figure 3c, 3d and 3e) and III (Figure 3f and 3 g). Within each group, when the solvothermal temperature and time were settled, and other conditions were identical, with the increase of the Eu^{3+} concentration, the size of the as-prepared nanorods decreased. From the TEM images of the as-prepared nanorods (Figure 3a and 3b), it is clear that the length of the nanorods rapidly elongated from ~110 nm (Figure 3b) to ~700−800 nm (Figure 3a) with the decrease of Eu^{3+} concentration from

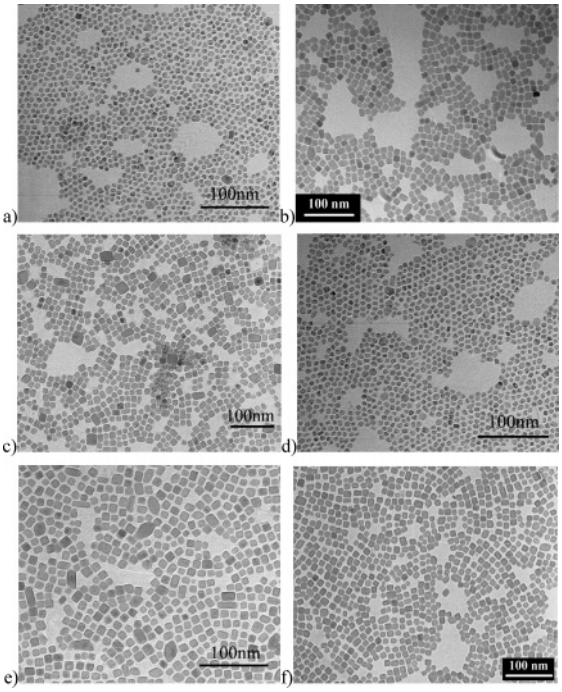

Figure 1. TEM images of the nanocrystals used to investigate the effect of NaF content on the morphology, size, and crystal structure of the as-prepared nanocrystals. All the samples are prepared under the conditions according to Table 1. TEM images for $NaYF_4$:Eu^{3+} nanocrystals prepared with the NaF/$Ln(NO_3)_3$ ratio of (a) 4, (b) 5, and (c) 10, respectively; TEM images for $NaYF_4$:Tb^{3+} nanocrystals prepared with the NaF/$Ln(NO_3)_3$ ratio of (d) 4, (e) 5, and (f) 10, respectively.

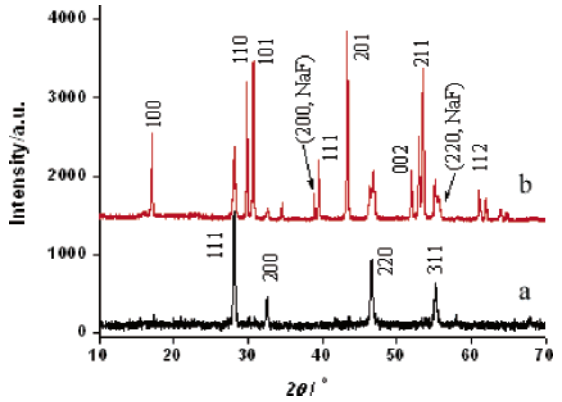

Figure 2. Powder XRD patterns of the as-prepared nanoparticles. (a) Irregular nanoparticles corresponding to samples in parts a and d of Figure 1 (cubic phase $NaYF_4$, JCPDS card 77-2042) and (b) regular nanocubes corresponding to nanocrystals in parts b, c, e, and f of Figure 1 (cubic phase and hexagonal phase $NaYF_4$ (JCPDS card 16-0334), excessive NaF also emerged).

71.4% (mol %; Figure 3b) to 28.6% (Figure 3a). Of course, when the doped Eu^{3+} reached 71.4%, the composition of the nanorods has changed from hexagonal phase $NaYF_4$ to hexagonal phase $NaEuF_4$, which have been identified by the following XRD patterns (Figure 4). Moreover, with the decrease in the content of Eu^{3+} from 28.6 to 5% (group II), the nanorods also elongated from ∼450−700 nm (Figure 3d) to ∼700−800 nm (Figure 3c), and the composition of the nanorods remained a hexagonal structure of $NaYF_4$, i.e. ,$Na(Y_{1.5}Na_{0.5})F_6$. In group III, the TEM images (images f and g of Figure 3) laid out more evidence that the doped ion content has a great effect on the morphology of the as-synthesized nanocrystals. Images f and g of Figure 3 depicted

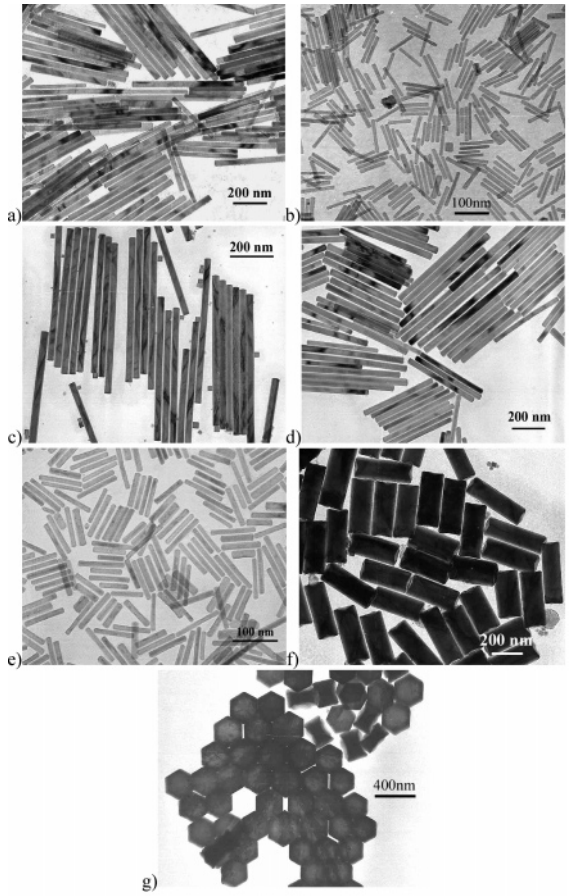

Figure 3. TEM images of the nanocrystals used to investigate the effect of doped Eu^{3+} concentration on the nanocrystals. All the samples were prepared under the conditions according to Table 2.

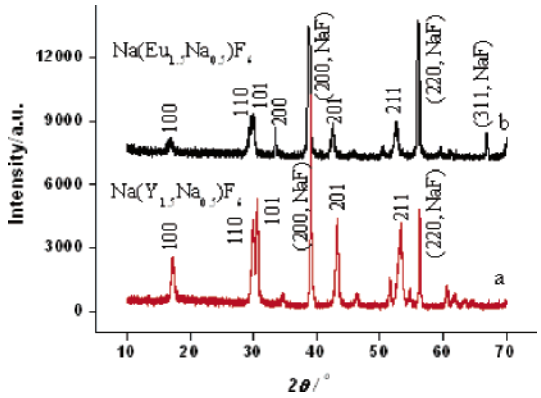

Figure 4. Powder XRD patterns of the as-prepared nanocrystals. (a) Hexagonal phase $NaYF_4$ nanorods corresponding to samples in Figure 3a; the samples of parts c, d, and f of Figure 3 have an XRD pattern similar to that for Figure 3a. (b) Hexagonal phase $NaEuF_4$ nanocrystals corresponding to samples in Figure 3b; the XRD pattern of parts e and g of Figure 3 is similar to that of Figure 3b; excessive NaF also emerged.

the different morphology of the nanocrystals prepared under the same conditions except for the Eu^{3+} concentration. All the as-synthesized nanocrystals have been characterized by XRD technology; however, for the sake of succinctness, only the XRD patterns of the nanocrystals doped with 28.6 (Figure 4a) and 71.4% (Figure 4b) Eu^{3+}, whose TEM images are depicted in images a and b of Figure 3, respectively, are given here. The XRD patterns of the nanorods (Figure 4a) were assigned to the <100>, <110>, <101>, <201>, and <211> reflections of the hexagonal structure of $NaYF_4$

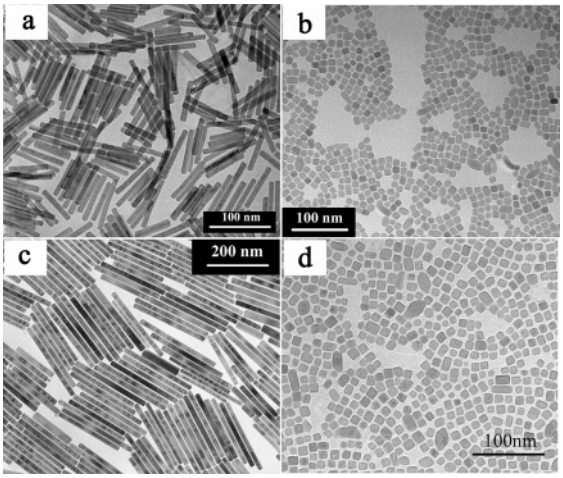

Figure 5. TEM images of the nanocrystals used to investigate the effect of the reactant concentration on the nanocrystals. Dopant is as follows: (a) 71.4% Eu^{3+}, (b) 5% Eu^{3+}, (c) 71.4% Tb^{3+}, (d) 5% Tb^{3+}. All the samples were prepared under the conditions according to Table 3.

(JCPDS card 16-0344). Meanwhile, the XRD patterns shown in Figure 4b confirmed the hexagonal structure of $NaEuF_4$ (JCPDS card 49-1897). Moreover, in the two sets of XRD patterns, unreacted NaF also emerged. Other nanocrystals demonstrated in Figure 3 and Table 2 have XRD patterns similar to that of hexagonal phase $NaYF_4$ when the doped Eu^{3+} concentration is <30% (images a, c, d, and f of Figure 3); however, when the Eu^{3+} concentration reaches 70%, the XRD pattern is identical to that of the hexagonal phase $NaEuF_4$ (images b, e, and g of Figure 3).

Effect of Reactant Concentration. By fixing other reaction conditions, the effect of the reactant concentration on the morphology and size of the as-prepared nanocrystals was investigated. Table 3 and Figure 5 clearly showed that low reactant concentration would result in nanorods. Under the same conditions despite different doped ions (Eu^{3+} or Tb^{3+}), when the reactant content (total amount of $Ln(NO_3)_3$) increased from 0.28 mmol (images a and c of Figure 5) to 0.60 mmol (images b and d of Figure 5), the acquired nanocrystals had completely different shapes and sizes. As shown in Figure 5, high reactant concentration preferably results in nanoparticles (images b and d of Figure 5), whereas low reactant concentration will lead to nanorods (images a and c of Figure 5). Although the nanorods preferably result from the high ratio of Y^{3+}/Eu^{3+} (or Y^{3+}/Tb^{3+}), which has been confirmed by the results in Table 2 and Figure 3, the high ratio of Y^{3+}/Eu^{3+} or Y^{3+}/Tb^{3+} here (images b and d of Figure 5) did not result in nanorods, which powerfully approved that the reactant content has obvious effects on the morphology and size of the as-synthesized nanocrystals.

Effect of Synthetic Temperature and Time. The effect of solvothermal temperature and time has also been investigated with upconversion luminescent $NaYF_4$ nanocrystals as examples in this work. Table 4 listed the experimental parameters and results in detail. As shown in Table 4 and images a and b of Figure 6, a higher temperature will decrease the length-to-diameter ratio of the as-prepared nanorods. However, to obtain nanorods instead of nanoparticles, we need adequate solvothermal time and temperature, which has been testified by the results depicted in images b and c of Figure 6. Too short of a reaction time resulted in only nanoparticles instead of nanorods (Figure 6c). Although excessive NaF is favorable for the epitaxial growth of $NaYF_4$ nanocrystals, as long as temperature and time are appropriately adopted (Figure 6d), nanorods have also been synthesized even when the ratio of $NaF/Ln(NO_3)_3$ is stoichiometric (i.e., four). These results indicate that the synthetic temperature and time have obvious effects on the nanocrystals. Moreover, just as shown above, in this $NaYF_4$:Yb^{3+}/Er^{3+} system, when the solvothermal temperature and time are identical, low reactant content and excessive NaF are preferable for the formation of nanorods (see Table 4, Figure 6d−f). Within the settled solvothermal time, low reactant content results in 100% nanorods (Figure 6f); meanwhile, high reactant content results in a mixture of nanorods and nanoparticles (Figure 6e). Corresponding XRD patterns of the as-prepared nanocrystals under the experimental conditions listed in Table 4 are given in this work. As shown in Figure 7, the XRD results indicate that the nanorods depicted in images d and e of Figure 6 are indexed to hexagonal phase $NaYF_4$ (JCPDS card 16-0334) although sometimes faint signals of excessive NaF and a small amount of cubic phase $NaYF_4$ emerged. Other nanorods demonstrated in Figure 6 are all assigned to hexagonal phase $NaYF_4$ (JCPDS card 16-0334; not shown here). The XRD patterns exhibited the <111>, <200> (shown in the Figure 7a), and <311> (shown in Figure 7b) peaks, which could be assigned to the <111>, <220>, and <311> reflections of face-centered cubic $NaYF_4$. Meanwhile, the nanoparticles of Figure 6c are assigned to cubic phase $NaYF_4$ (JCPDS card 77-2042), and the XRD pattern was similar to that in Figure 2a with some excess NaF (pattern not shown here). Experimental results indicated that the excess NaF can be removed

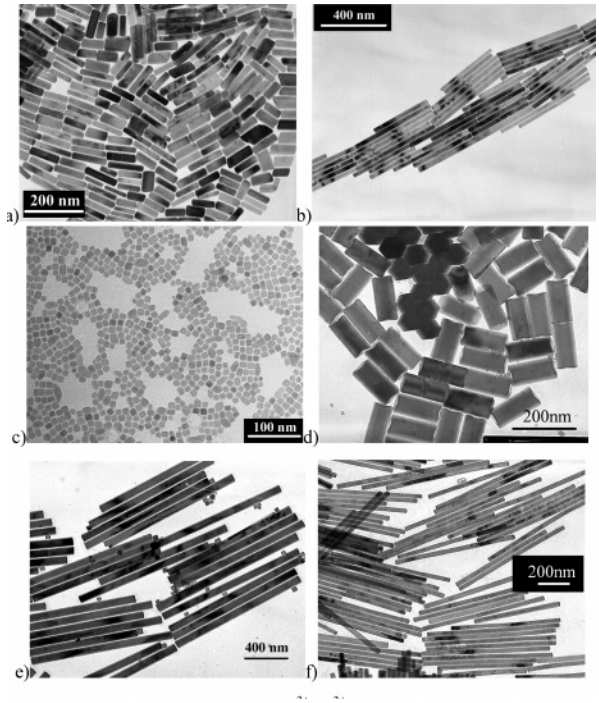

Figure 6. TEM images of the $NaYF_4$:Yb^{3+}/Er^{3+} nanocrystals used to investigate the effect of the reaction temperature and time on the morphology and size of the nanocrystals. All the samples are prepared under the conditions according to Table 4.

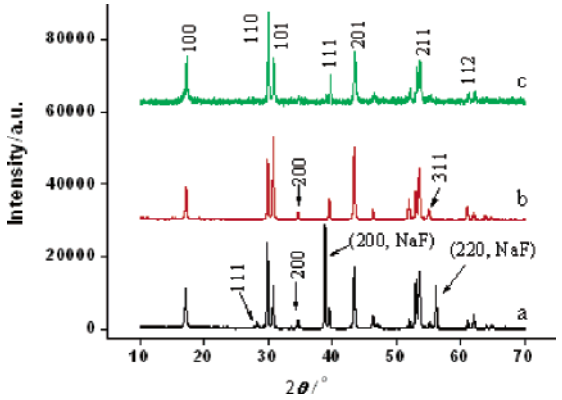

Figure 7. XRD patterns of the as-prepared nanocrystals depicted in Figure 6. (a) Nanocrystals of Figure 6e with a small amount of cubic $NaYF_4$ and excessive NaF; (b) nanocrystals of Figure 6d with some cubic $NaYF_4$ but without NaF; (c) nanocrystals of Figure 6f after removing the excess NaF by washing with water or purifying with filtration without water washing.

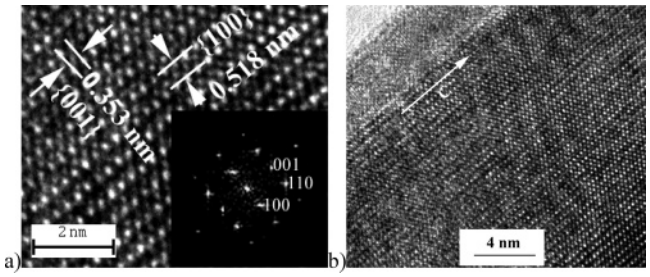

Figure 8. HRTEM of the $NaYF_4$ nanorods (a) showing that the growth direction is along the <001> surface (inset of (a) is the Fourier transform of the HRTEM image), and (b) showsing the surfaces of the nanorods covered with surfactants (oleic acids). These 5% Eu^{3+} doped $NaYF_4$ nanorods are prepared at 190 °C for 24 h.

by washing with water or filtrating and washing with ethanol (see XRD pattern in Figure 7c).

Formation Mechanism of the Nanorods. The above experimental results demonstrate that high Y^{3+}/Ln^{3+} ratio (here, Ln^{3+} represents the doped ions), low reactant concentration (the total amount of $Y(NO_3)_3$ and doped ions), high NaF content, long synthetic time, and appropriate solvothermal temperature are favorable for the formation of nanorods. Meanwhile, all the results indicate that the formation mechanism of the nanorods is so complicated that there is no single factor that can decide the morphology and size of the as-prepared nanocrystals. To the best of our knowledge, selective adhesion of surfactants is critical in the epitaxial growth of nanocrystals.[34,35] In this work, we speculate that during the growth of $NaYF_4$ nanocrystals, the surfactants (oleic acids) selectively bind to the surfaces that are parallel to the *c*-axis of the growing crystallites, which renders the epitaxial growth along the <001> directions and results in nanorods. The high-resolution transmission electron microscopy (HRTEM) image (Figure 8a) clearly shows that the epitaxial growth is along the <001> surfaces. Meanwhile, from Figure 8b, the selectively adhered oleic acids on the surfaces can also be seen, which identified our speculation.

DC and UC Photoluminescence of the As-Prepared Nanocrystals. Room-temperature downconversion luminescence spectra of the Tb^{3+}- (Figure 9a) and Eu^{3+}-doped (Figure 9b) $NaYF_4$ nanocrystals are shown here. Under 220 nm excitation, the $NaYF_4$:Tb^{3+} nanocrystals with a doping concentration of 5% show the typical emission peaks of terbium at 486, 543, 587, and 619 nm assigned to the $^5D_4-{}^7F_J$ ($J = 6, 5, 4, 3$) transition (Figure 9a), respectively.[25] The dominant green emission band corresponding to the $^5D_4-{}^7F_5$ peak is around 543 nm. The emission spectrum depicted here starts from 450 nm to avoid an excitation peak near 440 nm (double excitation) and thereby depict the emission peaks clearly. Figure 9b shows the room-temperature fluorescence spectra of Eu^{3+}-doped $NaYF_4$ nanocrystals excited at different wavelengths. As shown in Figure 9b, the DC luminescence changed greatly with the alteration of excitation wavelength. As we know, energy transfer from host materials or other ions with a higher absorption coefficient could lead to much more efficient luminescence.[36] Just as charge-transfer transition in the Ln−O bond in Eu^{3+}-doped $LaPO_4$ nanoparticles, the energy transfer in the Ln−F bond in the as-prepared Eu^{3+}-doped $NaYF_4$ nanocrystals may contribute to the luminescence. To obtain the strong red DC emission centered at ~610 nm, we need the optimal excitation of $NaYF_4$: Eu^{3+} nanocrystals to be around 265 nm, which may be adjacent to the efficient absorption wavelength for the Ln−F bond, whereas, if the split lines of the typical emission of Eu^{3+} is desired, the 375 nm excitation light should be chosen. An interesting feature is that the typical emission peaks of Eu^{3+} around the range of 580−660 nm are interlaced under 265 nm excitation. Only excited at 375 nm, the split fluorescence peaks of Eu^{3+} are clear. As shown in the inset (b1) of Figure 9b, the emission spectra of a $NaYF_4$:Eu^{3+} cyclohexane solution shows strong peaks at 594 and 614 nm that are attributable to the $^5D_0-{}^7F_1$ and $^5D_0-{}^7F_2$ transitions, respectively.[25,37]

Figure 9c shows the unique upconversion fluorescence spectra of $NaYF_4$:Yb^{3+}/Er^{3+} and $NaYF_4$:Yb^{3+}/Tm^{3+} nanocrystals with a 0−800 mW adjustable 980 nm laser. The three emissions of $NaYF_4$:Yb^{3+}/Er^{3+} nanocrystals (green solid line in Figure 9c) are attributed to the transitions $^2H_{11/2}-{}^4I_{15/2}$ (~519 nm), $^4S_{3/2}-{}^4I_{15/2}$ (~541 nm) and $^4F_{9/2}-{}^4I_{15/2}$ (~653 nm) for the Er^{3+} ions.[17−19,26] The most intense green emission line is located at 541 nm. The blue upconversion of $NaYF_4$:Yb^{3+}/Tm^{3+} nanocrystals obtained for excitation of the 980 nm is also depicted with a dotted line in Figure 9c (blue dash line). In this case, the emission (449 nm) from $^1D_2$ to $^3H_6$ ($^1D_2-{}^3H_6$) is very weak. The main emission of blue luminescence (470 nm) arises from the $^1G_4-{}^3H_6$ energy transition of the Tm^{3+} ion. The red emission located at 647 nm can be assigned to the $^1D_2-{}^3F_4$ energy transition.[20,21] Inset c1 in Figure 9c is the naked-eye-visible blue UC emission pattern of $NaYF_4$:Yb^{3+}/Tm^{3+} nanocrystals dissolved in cyclohexane under 980 nm excitation. Meanwhile, the inset c2 of Figure 9c is the naked-eye-visible green UC emission

(34) Manna, L.; Scher, E. C.; Alivisatos, A. P. *J. Am. Chem. Soc.* **2000**, *122*, 12700.
(35) Peng, Z. A.; Peng, X. G. *J. Am. Chem. Soc.* **2002**, *124*, 3343.
(36) Stouwdam, J. W.; Raudsepp, M.; van Veggel, F. *Langmuir* **2005**, *21*, 7003.
(37) Yan, R. X.; Sun, X. M.; Wang, X.; Peng, Q.; Li, Y. D. *Chem.—Eur. J.* **2005**, *11*, 2183.

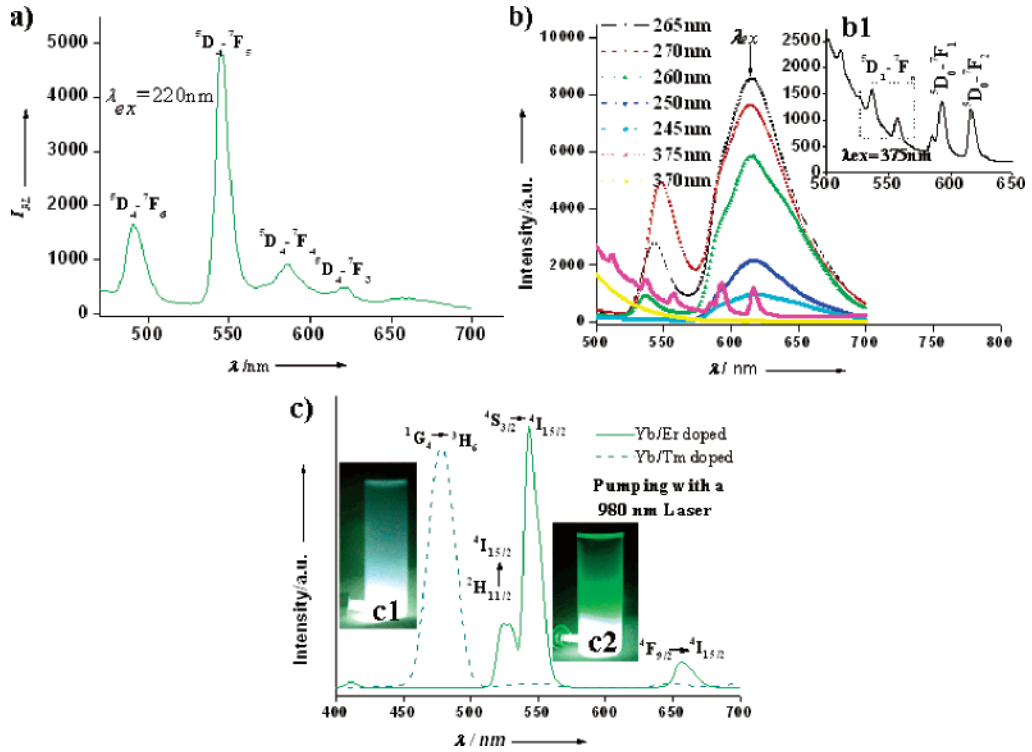

Figure 9. Room-temperature fluorescence spectra and luminescence photos of the as-prepared nanocrystals. (a) Fluorescence emission spectrum of $NaYF_4$:Tb^{3+} nanocrystals excited at ~220 nm; (b) fluorescence spectra of $NaYF_4$:Eu^{3+} nanocrystals at different excitation wavelengths (inset (b1) is the high-resolution fluorescence spectrum of $NaYF_4$:Eu^{3+} nanocrystals excited at 375 nm); (c) upconversion fluorescence spectra of $NaYF_4$:Yb^{3+}/Tm^{3+} (left, blue dash line) and $NaYF_4$:Yb^{3+}/Er^{3+} (right, green solid line) nanocrystals excited under 980 nm (inset (c1) is the blue UC emission photo of $NaYF_4$:Yb^{3+}/Tm^{3+} nanocrystals dissolved in cyclohexane under 980 nm excitation) inset (c2) is the green UC emission photo of $NaYF_4$:Yb^{3+}/Er^{3+} nanocrystals dissolved in cyclohexane under 980 nm excitation.

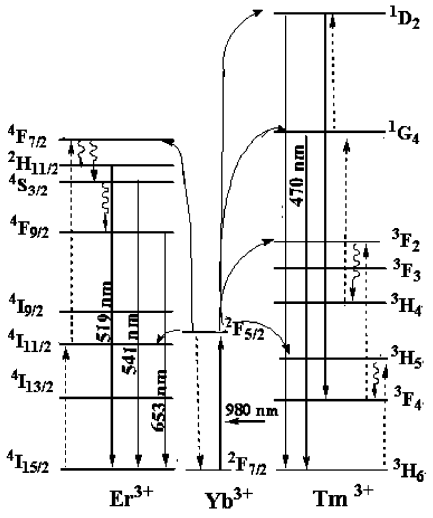

Figure 10. Schematic energy-level diagrams, upconversion excitation, and visible emission schemes for the Yb^{3+}−Er^{3+} and Yb^{3+}−Tm^{3+} systems.

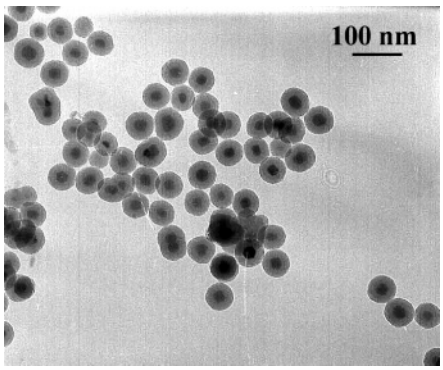

Figure 11. TEM image of the SiO_2-coated $NaYF_4$ nanoparticles.

photo of $NaYF_4$:Yb^{3+}/Er^{3+} nanocrystals dissolved in cyclohexane pumped with 980 nm laser. The resulted upconversion emissions indicate that both $NaYF_4$:Yb^{3+}/Er^{3+} and $NaYF_4$:Yb^{3+}/Tm^{3+} nanocrystals possess novel monochromatic properties, which is preferable for the discrimination of different labels for multicomponent simultaneous biodetection in complicated biological systems.

Upconversion Luminescence Mechanism of the Nanocrystals. Upconversion is an effective avenue for the generation of visible emission with near-infrared (NIR) excitation, which is based on sequential photon absorption and energy transfer steps.[17,20,21,26] As shown in Figure 10, in the case of $NaYF_4$:Yb^{3+}/Er^{3+} nanocrystals, the generation of these transitions is possible because of an efficient energy-transfer process involving Yb^{3+}−Er^{3+} ions. Under the excitation of 980 nm light, which can be absorbed by Yb^{3+}, the electrons of Er^{3+} are first excited from the $^4I_{15/2}$ to the $^4I_{11/2}$ level ($^4I_{15/2}$−$^4I_{11/2}$, Er^{3+}) via excitation energy transfer from Yb^{3+} to Er^{3+} and then to the $^4F_{7/2}$ level ($^4I_{11/2}$−$^4F_{7/2}$, Er^{3+}) by absorbing the energy of another electron from Yb^{3+} ($^2F_{5/2}$). The excited electrons of the $^4F_{7/2}$ (Er^{3+}) level then decay to the emitting $^2H_{11/2}$, $^4S_{3/2}$, and $^4F_{9/2}$ levels, mainly through nonradiative process. Here, the $^4S_{3/2}$ level is predominantly excited in this material, observed for the high luminescence intensity of the $^4S_{3/2}$−$^4I_{15/2}$ transition (541 nm).

Meanwhile, in the case of $NaYF_4$:Yb^{3+}/Tm^{3+} nanocrystals, the energy-transfer mechanism is more complicated than that in $Yb^{3+}-Er^{3+}$ codoped $NaYF_4$ nanocrystals and has been depicted in Figure 10. In a first nonradiative energy-transfer step, an Yb^{3+} ion in the $^2F_{7/2}$ ground state absorbs a 980 nm photon and transits to excited state $^2F_{5/2}$ ($^2F_{7/2}-{}^2F_{5/2}$). When it drops back to the ground state ($^2F_{5/2}-{}^2F_{7/2}$), energy is transferred to an adjacent ground state ($^3H_6$) Tm^{3+} ion to create a $^3H_5$ excited state ($^3H_6-{}^3H_5$). In a stepwise upconversion process, up to four Yb^{3+} excitation photons are injected into Tm^{3+}. After multistep excitation energy transfer, the Tm^{3+} is promoted to the $^1D_2$ and $^1G_4$ emission levels. These excited electrons on the emitting levels ($^1D_2$ and $^1G_4$) then dropped back to the low-energy levels ($^3F_4$ and $^3H_6$) via fluorescence emission.

Surface Modification of the Nanoparticles. For the next bioapplication as fluorescence labels, the luminescent nanoparticles transparently dispersed in cyclohexane should be transferred into aqueous solution. As reverse microemulsion is a facile method for silica-coating synthesis and modification of nanoparticles,[11] herein, this novel method was applied to the surface modification of the oleic-acid-coated nanoparticles. Figure 11 shows the TEM images of the silica-coated nanoparticles, which will facilitate the bioapplications of these nanocrystals.

Conclusion

In summary, we have developed a facile solution route to preparing uniform and highly luminescent nanorods/nanoplates/nanoparticles starting from simple inorganic chemicals by solvothermal technology. The effects of synthetic conditions such as NaF content, $Ln(NO_3)_3$ content, dopant concentration, solvothermal temperature, and time on the nanocrystals have been demonstrated detailedly. Results indicate that high NaF content, low $Ln(NO_3)_3$ content, appropriate temperature, and long solvothermal time are preferable for the epitaxial growth of the $NaYF_4$ nanocrystals. Moreover, the resulting nanocrystals exhibit both upconversion and downconversion fluorescence at room temperature. Ongoing efforts are being directed to resolve the details of the formation mechanism for the nanocrystals and introduce these highly luminescent nanocrystals into bioapplications such as biolabels.

Acknowledgment. This work was supported by NSFC (50372030, 20131030, 90406003) and the State Key Project of Fundamental Research for Nanomaterials and Nanostructures (2003CB716901).

CM061887M